Implementation of Backpropagation Neural Network for Prediction Magnetocaloric Effect of Manganite

Jan Setiawan[1*], Silviana Simbolon[2], Yunasfi[3]

[1,3]*Research Center for Advanced Material, BRIN, Indonesia*
[1]*Department of Electrical Engineering, Pamulang University, Indonesia*
[2]*Department of Mechanical Engineering, Pamulang University, Indonesia*

*corr_author: jan.setiawan@brin.go.id

Abstract - In the field of magnetic cooling technology, there is still much to learn about the magnetocaloric properties of magnetic cooling materials. Research into magnetocaloric manganites exhibiting a significant maximum magnetic entropy change in the vicinity of ambient temperature yields encouraging outcomes for the advancement of magnetic refrigeration apparatus. Through a combination of chemical substitutions, changes in the amount of oxygen present, and different synthesis techniques, these manganites undergo lattice distortions that result in pseudocubic, orthorhombic, and rhombohedral structures instead of perovskite cubic structures. The present investigation used backpropagation neural networks (BPNNs) to investigate the correlations among maximum magnetic entropy change (MMEC), Curie temperature (Tc), lanthanum manganite compositions, lattice properties, and dopant ionic radii. Simbrain 3.07 was used to execute the BPNN model, and the suggested model accuracy was examined using coefficient determination. As a result, the model's predicted values for the mean absolute error, root mean square, and coefficient correlation for MMEC are 0.012, 0.022, and 0.9861, respectively. The model predicts that the Curie temperature mean absolute error, root mean square, and coefficient correlation will be 0.015, 0.021, and 0.9947, respectively. Based on these results, BPNN has the potential to be applied in predicting the MMEC and Tc of manganite as preliminary decision during experiments.

Keywords: backpropagation neural network, simbrain, manganites, magnetocaloric effect, Curie temperature

I. INTRODUCTION

The use of refrigeration has become a very common occurrence in modern society. Until now, the use of compressed refrigerant materials is still the main choice in cooling applications. Chlorofluorocarbons (CFCs) and hydrochlorofluorocarbons (HCFCs) are refrigerant materials that are not environmentally friendly. One solution is a magnetic refrigerant that can be used as an alternative to replace refrigerant materials that are pollutants and, in its use, does not require the use of compressors. Moreover, the magnitude of the cooling efficiency of magnetic refrigerant (MR) is higher than that of conventional refrigerants. This efficiency is visible even on a small scale, making it possible to make small, portable refrigeration devices that can use a battery power supply. MR materials do not produce releases that harm the environment, so this technology can be said to be environmentally friendly. MR materials have been applied in various industries and commercial refrigeration, such as air conditioning, heat exchangers, waste separation, and others [1]. Research that focuses on exploring extraordinary characteristics such as colossal magnetoresistance (CMR) and magnetocaloric effect (MCE) in the ferromagnetic-paramagnetic phase transition temperature range is still a trending topic in the field of condensed matter. MCE characteristics are intrinsic properties of a magnetic material that can be utilized as a magnetic refrigerant. MR materials that are currently widely recognized are gadolinium and its alloys. Gadolinium and its alloys have magnetocaloric characteristics at room temperature but have the disadvantage that they are expensive and require a magnetic field of more than 5 T to operate, making them uneconomical [2]. Another alloy that has magnetocaloric characteristics at room temperature is lanthanum manganite. Manganite alloys generally have a formula that can be written as $R_{(1-x)}M_xMnO_3$, where R is a rare earth metal ion, and M is an alkaline earth divalent ion. The magnetocaloric material must have a Curie temperature (Tc) of close to room temperature and demonstrate a significant magnetic entropy change (ΔSm) over considerable temperature fluctuations in order to be fabricated into an operable magnetic refrigerator at room temperature. Manganite alloys have been researched for various applications such as magnetic refrigerants [3], catalysts [4], sensor applications [5], solid oxide fuel cell electrodes [6], hydrogen storage [7], solar cells [8] and biomedical [9]. Ferromagnetic lanthanum manganite with significant MCEs and useful Tc values has garnered much interest among candidates for magnetocaloric materials.

The Back Propagation Neural Network (BPNN) is one Artificial Neural Network model used to solve problems [10]. This model is employed because it can typically identify the necessary pattern and predict when the facts or phenomena will recur before they do. Although the architecture of the backpropagation network can theoretically have multiple hidden layers depending on system needs, it only has one hidden layer. On the other hand, the number of input and output patterns dictate how many vertices are connected to the input layer and the output layer. Finding the right weighting value is the goal of training a neural network. Many researchers have applied the concept of backpropagation from ANN in a material characteristic application, such as [11] and [12] have applied the backpropagation algorithm to predict the material's mechanical performance.

Experiments, mostly by varying synthesis methods (solid-state reaction, wet chemistry, and sol-gel), morphologies (particle size and shape), crystalline states, and final forms (powder, pellet, and film), have been used to examine the effect of dopant types and levels on the maximum magnetic entropy change (MMEC) of lanthanum manganites [13], [14]. Analysis has been done on manganites with a wide working temperature range and a large MCE around Tc [15]–[18]. This study presents a BPNN model for predicting the MMEC and Tc of manganite. The model utilizes lattice parameters and constituent elements, which can be readily obtained in the early stages of research. In the process of predicting, the statistical relationships between MMEC, Tc, compositions of manganites, lattice parameters, and ionic radii of dopants were examining through Pearson correlation coefficient (CC), mean absolute error (MAE), and root mean square error (RMSE) as the performance of the proposed model. Since certain descriptive features are present, the model generalizes well enough for intelligent algorithms to pick up on the patterns and recognize them. These effectively aid in the prediction of MMEC and Tc at low cost, and they may further our understanding of it through the use of lattice parameters, ionic radii, and compositions. One can use this model as a reference to find bulk manganites with promising MMEC and Tc. The model ought to be employed in machine learning to facilitate comprehension of magnetic phase transitions in various forms of doped manganite. Accurate forecasting of MMEC and Tc using this BPNN model will facilitate the design of manganite that is more effective, efficient and at a low cost based on its application.

II. METHOD

This research uses inputs of as many as 15 variables, with a total of 49 data used as training data and test data. The variables used consist of 3 variables of lattice parameters a, b, and c of the crystal structure, which can be obtained through Rietveld analysis or measurement. These lattice parameters have units in Angstrom that denoted by Å. Other variables are six groups of elemental composition that compose manganite consisting of lanthanide major, lanthanide minor, divalent elements, monovalent, transition metal or others, and additional elements. Each group of elemental composition variables consists of atomic radius and atomic fraction. Atomic radius has picometer units that denoted by pm and atomic fraction without units.

The processing group was varied into 1, 2, and 3 hidden layers with a total number of 45 nucleons. The first processing group has one hidden layer consisting of 45 nucleons (P1). The second variation for the processing group is two hidden layers with the formation of 15 nucleons and 30 nucleons (P2). The last variation uses three hidden layers containing 15 nucleons (P3). The BPNN was done in Simbrain 3.07, with the architecture illustration for P1 with one hidden layer in Fig. 1. The learning rate parameter used is 0.25, with a momentum of 0.9. The activation function used is binary sigmoidal. The activation function is a logistic function, and it can be differentiable with an output will vary around 0 to 1. The predicted outputs are two variables: maximum magnetic entropy change (MMEC) and Curie temperature (Tc). The data used for training and testing is given in Table I. Data for 15 variables were taken from the references listed respectively. The columns labelled a, b, and c represent the lattice parameters associated with the specific type of manganite material in the manganite column. The lanthanide major column provides data on the atomic radius and atomic fraction of the lanthanide element, which plays a key role in the formation of manganite. The lanthanide minor column gives data on the atomic radius and atomic fraction of the lanthanide element that partially substitutes the lanthanide major element. The divalent column consists data on the atomic radius and atomic fraction of elements that possess two valence electrons and can also serve as substitutes for the lanthanide major element. A monovalent column gives data on the atomic radius and atomic fraction of element that has only one valence electron and also substitutes the lanthanide major element. The transition metal or others column consist of transition metals or other elements that substitutes the manganese (Mn) element. The additional column contains data on the atomic radius and atomic fraction of an element that is neither divalent nor monovalent, even though it can serve as a substitute for the lanthanide elements.

TABLE I
EXPERIMENTAL DATA FOR MAXIMUM MAGNETIC ENTROPY CHANGE AND CURIE TEMPERATURE OF MANGANITE

No	Manganites	a	b	c	Major Lanthanide		Minor Lanthanide		Divalent		Monovalent		Transition metal or others		Additional		Experimental		References
					r	at	r	at	r	at	r	at	r	at	r	at	MMEC	Tc	
		(Å)	(Å)	(Å)	(pm)		(pm)		(pm)		(pm)		(pm)		(pm)		J/(Kg.K)	(K)	
1.	$(La_{0.56}Ce_{0.14})Sr_{0.3}MnO_3$	5.5037	5.5037	13.3452	112.6	0.56	119.6	0.14	131.0	0.30	0	0	0	0	0	0	4.78	357	[19]
2.	$La_{0.57}Nd_{0.1}Sr_{0.33}Mn_{0.95}Sn_{0.05}O_3$	5.4951	5.4951	13.3520	112.6	0.57	116.3	0.10	131.0	0.33	0	0	69.0	0.050	0	0	2.80	282	[20]
3.	$La_{0.57}Nd_{0.1}Sr_{0.33}Mn_{0.9}Sn_{0.1}O_3$	5.5394	5.5394	13.4236	112.6	0.57	116.3	0.10	131.0	0.33	0	0	69.0	0.100	0	0	3.22	224	[19]
4.	$La_{0.5}Sm_{0.2}Sr_{0.3}Mn_{0.8}Fe_{0.15}O_3$	5.5038	7.7388	5.4746	112.6	0.50	113.2	0.20	131.0	0.30	0	0	64.5	0.150	0	0	0.77	94	[21]
5.	$La_{0.5}Sm_{0.2}Sr_{0.3}Mn_{0.95}Fe_{0.05}O_3$	5.5036	7.7252	5.4678	112.6	0.50	113.2	0.20	131.0	0.30	0	0	64.5	0.050	0	0	2.93	253	[19]
6.	$La_{0.5}Sm_{0.2}Sr_{0.3}Mn_{0.9}Fe_{0.1}O_3$	5.5027	7.7403	5.4740	112.6	0.50	113.2	0.20	131.0	0.30	0	0	64.5	0.100	0	0	2.22	136	[22]
7.	$La_{0.5}Sm_{0.2}Sr_{0.3}MnO_3$	5.5019	7.7321	5.4696	112.6	0.50	113.2	0.20	131.0	0.30	0	0	0	0	0	0	3.06	278	[23]
8.	$La_{0.67}Ba_{0.33}Mn_{0.98}Ti_{0.02}O_3$	3.9119	3.9119	3.9119	112.6	0.67	0	0	147.0	0.33	0	0	60.5	0.020	0	0	3.24	314	[24]
9.	$La_{0.67}Ba_{0.33}MnO_3$	3.9075	3.9075	3.9075	112.6	0.67	0	0	147.0	0.33	0	0	0	0	0	0	1.48	350	[25]
10.	$La_{0.67}Ca_{0.33}Mn_{0.75}Cr_{0.25}O_3$	5.4419	7.6921	5.4608	112.6	0.67	0	0	118.0	0.33	0	0	61.5	0.250	0	0	2.20	189	[26]
11.	$La_{0.67}Ca_{0.33}Mn_{0.98}Ni0.02O_3$	5.4545	5.4545	13.3922	112.6	0.67	0	0	118.0	0.33	0	0	60.0	0.020	0	0	8.00	244	[20]
12.	$La_{0.67}Ca_{0.33}Mn_{0.9}Cr_{0.1}O_3$	5.4486	7.7000	5.4673	112.6	0.67	0	0	118.0	0.33	0	0	61.5	0.100	0	0	3.50	215	[27], [28]
13.	$La_{0.67}Sr_{0.33}MnO_3$	5.4879	5.4879	13.3622	112.6	0.67	0	0	131.0	0.33	0	0	0	0	0	0	5.15	375	[22]
14.	$La_{0.6}Pr_{0.1}Ba_{0.3}Mn_{0.7}Ni_{0.3}O_3$	5.4813	7.6853	5.4519	112.6	0.60	117.9	0.10	147.0	0.30	0	0	60.0	0.300	0	0	0.65	131	[29]
15.	$La_{0.6}Pr_{0.1}Ba_{0.3}Mn_{0.9}Ni_{0.1}O_3$	5.5032	7.7200	5.4690	112.6	0.60	117.9	0.10	147.0	0.30	0	0	60.0	0.100	0	0	1.31	162	[30]
16.	$La_{0.6}Pr_{0.1}Ba_{0.3}MnO_3$	5.5121	7.7508	5.4859	112.6	0.60	117.9	0.10	147.0	0.30	0	0	0	0	0	0	1.97	215	[29], [31]
17.	$La_{0.7}Ba_{0.3}MnO_3$	3.9084	3.9084	3.9084	112.6	0.70	0	0	147.0	0.30	0	0	0	0	0	0	2.70	335	[30], [32]
18.	$La_{0.7}Pb_{0.3}Mn_{0.8}Ru_{0.2}O_3$	5.5365	5.5365	13.4237	112.6	0.70	0	0	135.0	0.30	0	0	56.5	0.200	0	0	3.06	335	[23], [31]
19.	$La_{0.7}Pb_{0.3}Mn_{0.9}Ru_{0.1}O_3$	5.5372	5.5372	13.4117	112.6	0.70	0	0	135.0	0.30	0	0	56.5	0.100	0	0	3.15	313	[29]
20.	$La_{0.7}Pb_{0.3}MnO_3$	5.5176	5.5176	13.4116	112.6	0.70	0	0	135.0	0.30	0	0	0	0	0	0	3.17	336	[20]
21.	$La_{0.7}Sr_{0.25}Na_{0.05}Mn_{0.8}Ti_{0.2}O_3$	5.5312	5.5312	13.4161	112.6	0.70	0	0	131.0	0.25	124.0	0.05	60.5	0.200	0	0	2.03	125	[33]
22.	$La_{0.7}Sr_{0.25}Na_{0.05}Mn_{0.9}Ti_{0.1}O_3$	5.5271	5.5271	13.4021	112.6	0.70	0	0	131.0	0.25	124.0	0.05	60.5	0.100	0	0	2.38	155	[23]
23.	$La_{0.7}Sr_{0.25}Na_{0.05}MnO_3$	5.5062	5.5062	13.3602	112.6	0.70	0	0	131.0	0.25	124.0	0.05	0	0	0	0	4.34	363	[29]
24.	$La_{0.7}Sr_{0.3}Mn_{0.9}Ti_{0.1}O_3$	5.5256	5.5256	13.3899	112.6	0.70	0	0	131.0	0.30	0	0	60.5	0.100	0	0	2.94	210	[34]
25.	$La_{0.7}Sr_{0.3}MnO_3$	5.4932	5.4932	13.3657	112.6	0.70	0	0	131.0	0.30	0	0	0	0	0	0	2.30	370	[20]
26.	$La_{0.7}Sr_{0.3}MnO_3$	5.4883	5.4883	12.3275	112.6	0.70	0	0	131.0	0.30	0	0	0	0	0	0	3.43	370	[35]
27.	$Nd_{0.67}Ba_{0.33}Mn_{0.98}Fe_{0.02}O_3$	5.4917	7.7602	5.5196	116.3	0.67	0	0	147.0	0.33	0	0	64.5	0.020	0	0	2.97	131	[29]
28.	$Nd_{0.67}Ba_{0.33}MnO_3$	5.4915	7.7591	5.5519	116.3	0.67	0	0	147.0	0.33	0	0	0	0	0	0	3.91	150	[25]
29.	$Pr_{0.3}Sm_{0.25}Sr_{0.45}MnO_3$	5.4623	5.4387	7.6779	117.9	0.30	113.2	0.25	131.0	0.45	0	0	0	0	0	0	4.92	225	[36]
30.	$Pr_{0.4}Sm_{0.15}Sr_{0.45}MnO_3$	5.4718	5.4399	7.6773	117.9	0.40	113.2	0.15	131.0	0.45	0	0	0	0	0	0	3.98	261	[35]
31.	$Pr_{0.6}La_{0.2}Sr_{0.2}MnO_3$	5.4937	5.4634	7.7656	117.9	0.60	112.6	0.20	131.0	0.20	0	0	0	0	0	0	2.17	150	[35]
32.	$Pr_{0.6}Sr_{0.3}Ca_{0.1}Mn_{0.025}Fe_{0.075}O_3$	5.4427	5.4669	7.6919	117.9	0.60	0	0	131.0	0.30	0	0	64.5	0.075	118.0	0.10	3.12	112	[25]
33.	$Pr_{0.7}Ca_{0.3}Mn_{0.08}Co_{0.02}O_3$	5.4303	7.6729	5.4599	117.9	0.70	0	0	118.0	0.30	0	0	54.0	0.020	0	0	2.18	106	[30], [32]
34.	$Pr_{0.7}Ca_{0.3}Mn_{0.95}Co_{0.05}O_3$	5.4299	7.6696	5.4572	117.9	0.70	0	0	118.0	0.30	0	0	54.0	0.050	0	0	2.96	105	[21]
35.	$Pr_{0.7}Ca_{0.3}Mn_{0.95}Co_{0.05}O_3$	5.4314	7.6711	5.4591	117.9	0.70	0	0	118.0	0.30	0	0	54.0	0.050	0	0	3.10	105	[37]
36.	$Pr_{0.7}Ca_{0.3}Mn_{0.95}Cr_{0.05}O_3$	5.4300	7.6679	5.4572	117.9	0.70	0	0	118.0	0.30	0	0	61.5	0.050	0	0	2.76	140	[37]
37.	$Pr_{0.7}Ca_{0.3}Mn_{0.95}Cr_{0.05}O_3$	5.4300	7.6679	5.4572	117.9	0.70	0	0	118.0	0.30	0	0	61.5	0.050	0	0	2.92	140	[38]
38.	$Pr_{0.7}Ca_{0.3}Mn_{0.95}Fe_{0.05}O_3$	5.4321	7.6743	5.4648	117.9	0.70	0	0	118.0	0.30	0	0	64.5	0.050	0	0	2.39	90	[26]
39.	$Pr_{0.7}Ca_{0.3}Mn_{0.95}Ni_{0.05}O_3$	5.4295	7.6708	5.4508	117.9	0.70	0	0	118.0	0.30	0	0	60.0	0.050	0	0	3.10	110	[24]
40.	$Pr_{0.7}Ca_{0.3}Mn_{0.9}Co_{0.1}O_3$	5.4306	7.6705	5.4484	117.9	0.70	0	0	118.0	0.30	0	0	54.0	0.100	0	0	3.20	116	[34]
41.	$Pr_{0.7}Ca_{0.3}Mn_{0.9}Cr_{0.1}O_3$	5.4293	7.6691	5.4552	117.9	0.70	0	0	118.0	0.30	0	0	61.5	0.100	0	0	2.81	150	[39]
42.	$Pr_{0.7}Ca_{0.3}Mn_{0.9}Fe_{0.1}O_3$	5.4319	7.6753	5.4646	117.9	0.70	0	0	118.0	0.30	0	0	64.5	0.100	0	0	2.10	80	[24], [40]
43.	$Pr_{0.7}Ca_{0.3}Mn_{0.9}Ni_{0.1}O_3$	5.4328	7.6892	5.4195	117.9	0.70	0	0	118.0	0.30	0	0	60.0	0.100	0	0	2.94	118	[22]
44.	$Pr_{0.8}K_{0.15}Na_{0.05}MnO_3$	5.5641	5.4661	7.7374	117.9	0.80	0	0	0	0	155.0	0.15	0	0	124.0	0.05	3.31	134	[41]
45.	$Pr_{0.8}Na_{0.2}MnO_3$	5.4460	5.4481	7.7113	117.9	0.80	0	0	0	0	124.0	0.20	0	0	0	0	3.40	92	[39]
46.	$Pr_{0.8}Na_{0.2}MnO_3$	5.4483	5.4359	7.6855	117.9	0.80	0	0	0	0	124.0	0.20	0	0	0	0	5.35	92	[42]
47.	$Pr_{0.8}Sr_{0.2}MnO_3$	5.4893	5.4795	7.7413	117.9	0.80	0	0	131.0	0.20	0	0	0	0	0	0	3.54	150	[37], [43]
48.	$Pr_{0.8}Sr_{0.2}MnO_3$	5.4711	7.7333	5.4858	117.9	0.80	0	0	131.0	0.20	0	0	0	0	0	0	4.09	150	[39]
49.	$Sm_{0.45}Pr_{0.1}Sr_{0.45}MnO_3$	5.4427	5.4415	7.6800	113.2	0.45	117.9	0.10	131.0	0.45	0	0	0	0	0	0	7.14	132	[44]

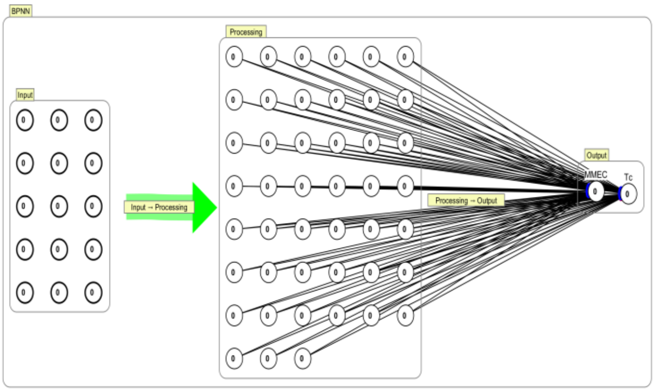

Fig. 1 Backpropagation neural network architecture (P1) for predicting manganite magnetocaloric effect and Curie temperature

The training was stopped when the iterations reached 10000. The performance of BPNN is evaluated by mean absolute error (MAE), root mean square error (RMSE), and correlation coefficient (CC) given by the following (1-3) [45], [46].

$$MAE = \frac{1}{n}\sum_{i=1}^{n}\left|x_i^{exp} - x_i^{pred}\right| \quad (1)$$

$$RMSE = \sqrt{\frac{1}{n}\sum_{i=1}^{n}\left(x_i^{exp} - x_i^{pred}\right)^2} \quad (2)$$

$$CC = \frac{\sum_{i=1}^{n}\left(x_i^{exp} - \overline{x^{exp}}\right)\left(x_i^{pred} - \overline{x^{pred}}\right)}{\sqrt{\sum_{i=1}^{n}\left(x_i^{exp} - \overline{x^{exp}}\right)^2 \sum_{i=1}^{n}\left(x_i^{pred} - \overline{x^{pred}}\right)^2}} \quad (3)$$

whereas n is the total number of data, x_i^{exp} is the i-th experimental data for MMEC and Tc, and its average value is $\overline{x^{exp}}$. The i-th predicted value for MMEC and Tc is denoted by x_i^{pred}, and its average value is $\overline{x^{pred}}$. The interpretation for the correlation coefficient given in Table II [47].

In order to forecast an unknown data for MMEC and Tc values, a set of manganites was synthesized using the composition specified in Table III. Manganite is produced through the powder metallurgy method, which involves mixing La_2O_3 powder, MnO_2 powder, $SrCO_3$ powder, and NiO powder in the correct composition. The powder mixture undergoes a 5-hour milling process followed by a 12-hour heating process at a temperature of 1200°C. The manganite that formed was analysed using X-ray diffraction, utilizing a PANalytical X-ray diffractometer equipped with a copper anode. The diffraction data obtained from manganite was examined using the General Structure Analysis Software (GSAS) application, which utilizes the Rietveld method to estimate the lattice parameters. The lattice parameters a, b and c that derived from GSAS, as well as the radius data and atomic fraction of the constituent elements of manganite, are provided in Table III. This value was tested on P1, P2 and P3 model to determined MMEC and Tc value.

TABLE II
INTERPRETATION FOR CORRELATION COEFFICIENT

Correlation coefficient	Interpretation
0.9 – 1	Very high
0.7 – 0.899	High
0.4 – 0.699	Enough
0.2 – 0.399	Low
< 0.2	Very low

TABLE III
EXPERIMENTAL DATA OF MANGANITE WITH UNKNOWN MAXIMUM MAGNETIC ENTROPY CHANGE AND CURIE TEMPERATURE FOR TESTING

No	Manganites	a	b	c	Major Lanthanide		Minor Lanthanide		Divalent		Monovalent		Transition metal or others		Additional	
					r	at	r	at	r	at	r	at	r	at	r	at
		(Å)	(Å)	(Å)	(pm)		(pm)		(pm)		(pm)		(pm)		(pm)	
1.	$LaMnO_3$	5.52523	5.52523	13.36977	112.6	1	0	0	131	0	0	0	0	0	0	0
2.	$La_{0.9}Sr_{0.1}MnO_3$	5.52649	5.52649	13.35858	112.6	0.9	0	0	131	0.1	0	0	0	0	0	0
3.	$La_{0.7}Sr_{0.3}MnO_3$	5.49928	5.49928	13.35068	112.6	0.7	0	0	131	0.3	0	0	0	0	0	0
4.	$La_{0.5}Sr_{0.5}MnO_3$	5.46575	5.46575	13.36132	112.6	0.5	0	0	131	0.5	0	0	0	0	0	0
5.	$La_{0.7}Sr_{0.3}Mn_{0.9}Ni_{0.1}O_3$	5.45398	5.45398	13.33506	112.6	0.7	0	0	131	0.3	0	0	60.0	0.1	0	0
6.	$La_{0.7}Sr_{0.3}Mn_{0.7}Ni_{0.3}O_3$	5.45066	5.45066	13.27469	112.6	0.7	0	0	131	0.3	0	0	60.0	0.3	0	0
7.	$La_{0.7}Sr_{0.3}Mn_{0.5}Ni_{0.5}O_3$	5.42494	5.42494	13.30135	112.6	0.7	0	0	131	0.3	0	0	60.0	0.5	0	0
8.	$La_{0.7}Sr_{0.3}Mn_{0.3}Ni_{0.7}O_3$	5.47675	5.47675	13.24651	112.6	0.7	0	0	131	0.3	0	0	60.0	0.7	0	0

III. RESULT AND DISCUSSION

A set of 49 data is given to each BPNN processing group in the form of inputs that consist of 15 variables and outputs as many as two variables. The training process was carried out as high as 10,000 iterations, and the amount of RMSE for the training data was given in Table IV. The sensitivity of BPNN for the predicted values that calculated using (1), (2) and (3) at different hidden layers in the processing group is given in Table IV as well.

The formation of the hidden layer affects the sensitivity of the BPNN so that the value obtained from the prediction is closer to the experimental data. In P1, the correlation coefficient values for MMEC and Tc are the best compared to P2 and P3. However, all of the correlation coefficients for P1, P2, and P3 show an interpretation in the very high category. The predicted values of Tc in P2 and P3 for MAE and RMSE values are slightly lower than those of P1. For more details, the comparison of predicted values with experimental data is described in Fig. 2 to Fig. 5. The very high correlation coefficient between the predicted and experimental data MMEC and Tc, the low prediction root mean square error and mean absolute error, and stable model performance suggest the usefulness of BPNN modeling and understanding the relationship between among the input and output variables [48].

A comparison of the MMEC predicted values with the experimental data is given in Figure 2. It can be seen that the predicted values are close to the experimental data. Significant differences are seen at two points, which are both $Pr_{0.8}Na_{0.2}MnO_3$ manganite for all processing groups, although one predicted value is lower and the other higher compared to the experimental data. Another difference is for $Pr_{0.7}Ca_{0.3}Mn_{0.08}Co_{0.05}O_3$ manganite that, the prediction value became less far from the experimental data. Differences can also be seen for $La_{0.7}Pb_{0.3}MnO_3$ manganite; in P1, the prediction value is near the experimental data. For P2, the prediction value is below the experimental data, and for P3, it is above its experimental data.

TABLE IV
SENSITIVITIES OF BACKPROPAGATION NEURAL NETWORK

Code	Hidden layer nucleon formation	Training MSE at 10,000 iterations	Prediction					
			CC		MAE		RMSE	
			MMEC	Tc	MMEC	Tc	MMEC	Tc
P1	45	0.0005	0.9861	0.9947	0.012	0.015	0.022	0.021
P2	15-30	0.0006	0.9807	0.9945	0.014	0.010	0.026	0.020
P3	15-15-15	0.0006	0.9818	0.9942	0.012	0.010	0.025	0.020

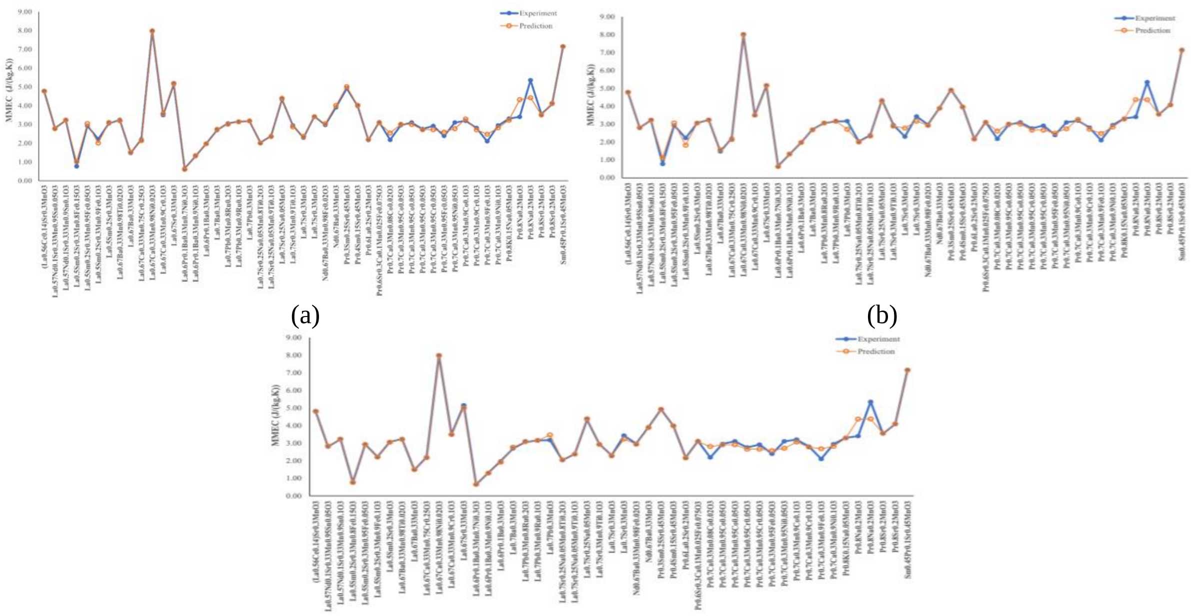

(c)

Fig. 2 Maximum magnetic entropy change for manganite, comparison prediction to experimental value (a) P1, (b) P2, and (c) P3

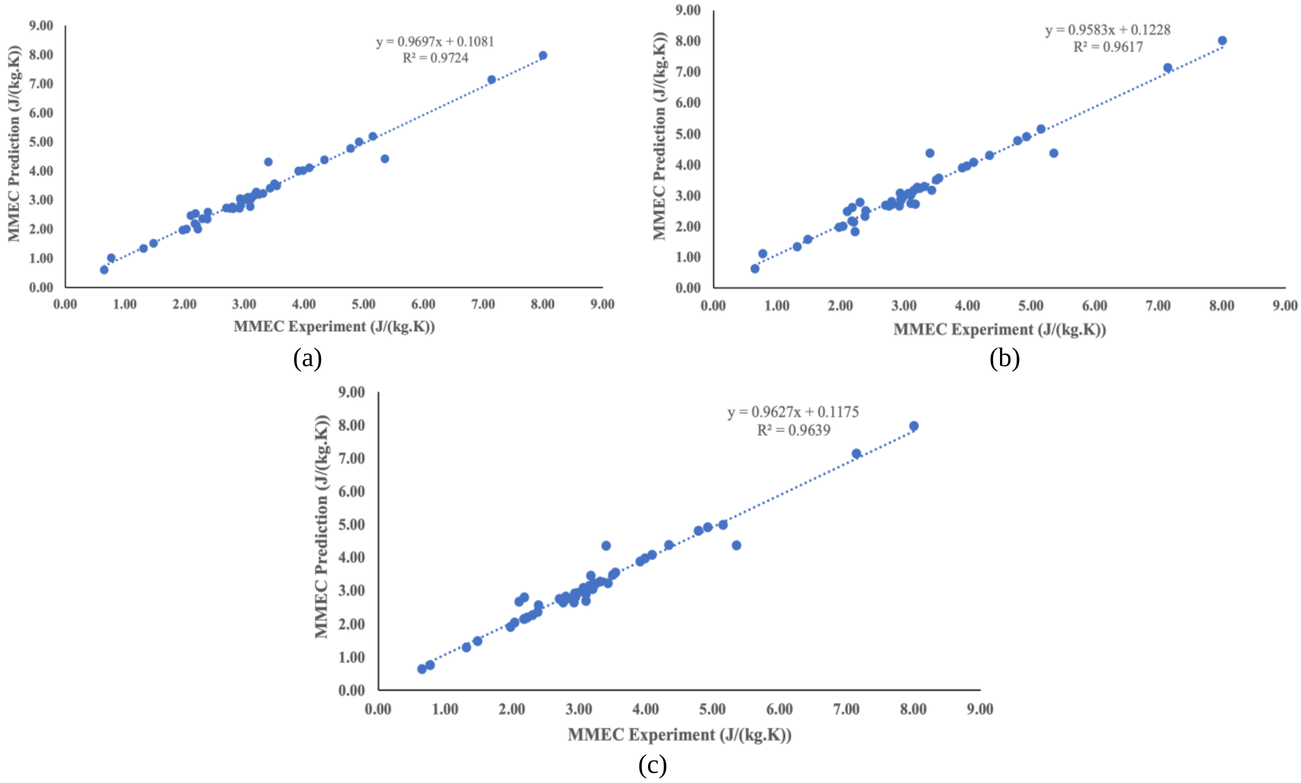

Fig. 3 Linearity correlation of predicted and experimental values for maximum magnetic entropy change (a) P1, (b) P2, and (c) P3

More details of the relationship between predicted values and experimental data of MMEC on manganite can be described through the linearity of the correlation. It can be seen that the data distribution is around the trendline with a good coefficient of determination (R^2) of 0.9724 for P1, 0.9617 for P2, and 0.9639 for P3. The value of the correlation coefficient (CC) for MMEC is given in Table IV. For manganite, which has a significant difference, it can be seen that the data points move away from the trendline.

Curie temperature predictions for each manganite are given in Figure 4. It can be seen that significant differences between predictions and experiments occur in five types of manganites for P1. Two data for the same type of manganite, namely $Pr_{0.7}Ca_{0.3}Mn_{0.95}Cr_{0.05}O_3$, then $Pr_{0.7}Ca_{0.3}Mn_{0.9}Cr_{0.1}O_3$, which are the three types of manganites, the predicted value is lower than the experimental data. Meanwhile, the manganite types $Pr_{0.7}Ca_{0.3}Mn_{0.95}Fe_{0.05}O_3$ and $Pr_{0.7}Ca_{0.3}Mn_{0.9}Fe_{0.1}O_3$ have higher predicted values than their experimental data. The prediction becomes better for Curie temperature, as seen for P2 and P3.

The linearity of the predicted value and experimental data of Curie temperature is given in Figure 5. The straight trendline has a good coefficient of determination (R^2) of 0.9893 for P1, 0.9890 for P2, and 0.9885 for P3. Thus, the correlation coefficient (CC) is given in Table IV. There are visible data points from manganite with significant differences in predicted value and experimental data. The manganite data points with relatively large value differences move away from the straight trendline. Of the three processing models seen to be able to show good accuracy to predict the value of MMEC and Tc. This model can be used to generalize the preparation of manganite to obtain a material with the desired maximum magnetic entropy change and Curie temperature. Thus, it will minimize the cost of developing manganite magnetic materials.

Furthermore, the P1, P2, and P3 models performed testing using the data provided in Table III. Figure 6 presents a comparison of the prediction outcomes obtained for MMEC and Tc.

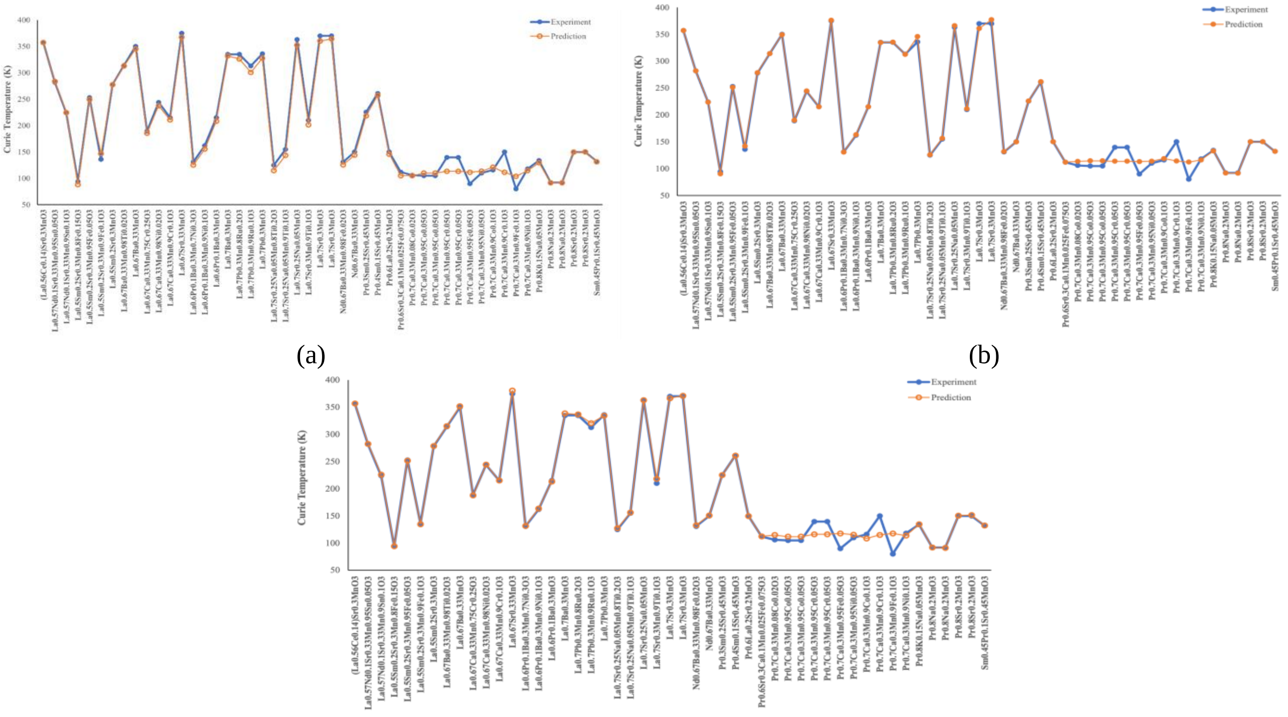

(c)

Fig. 4 Curie temperature for manganite, comparison prediction to experimental value (a) P1, (b) P2, and (c) P3

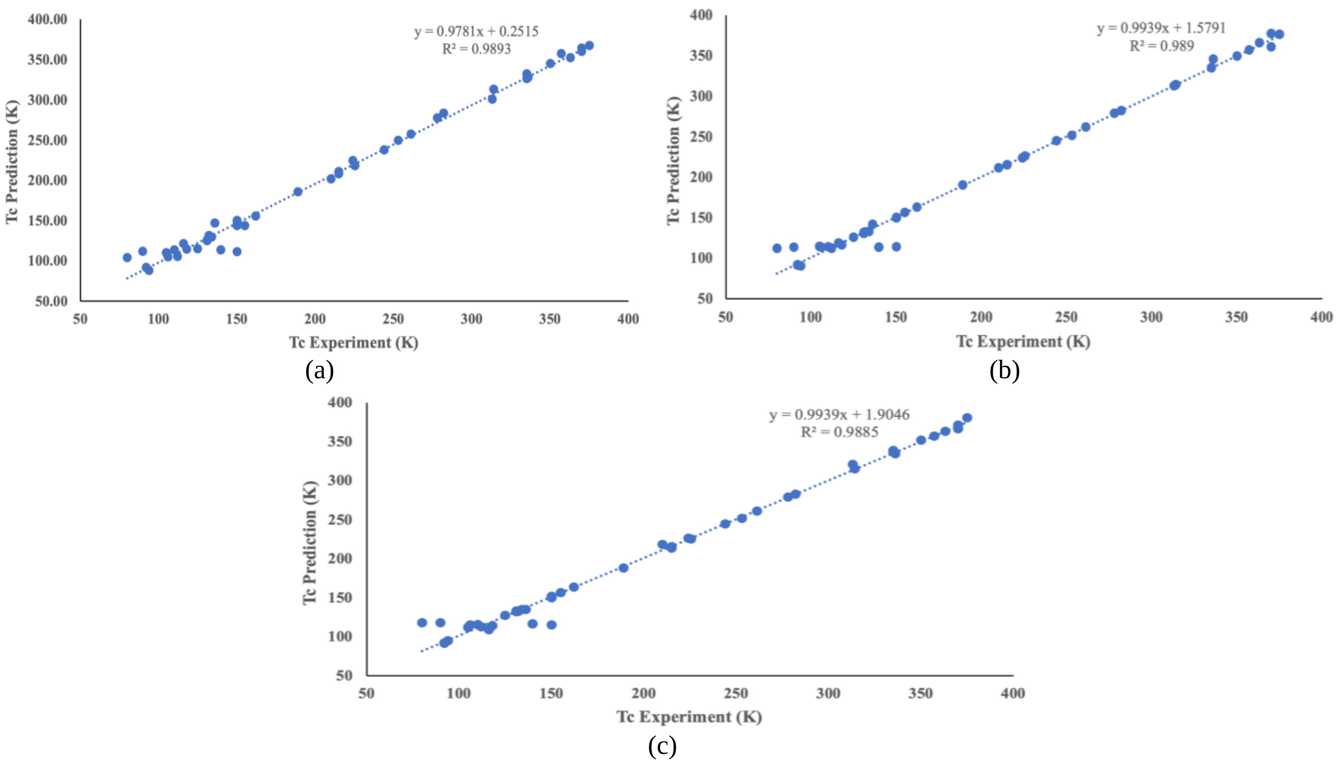

(c)

Fig. 5 Linear correlation of predicted and experimental values for Curie temperature (a) P1, (b) P2, and (c) P3

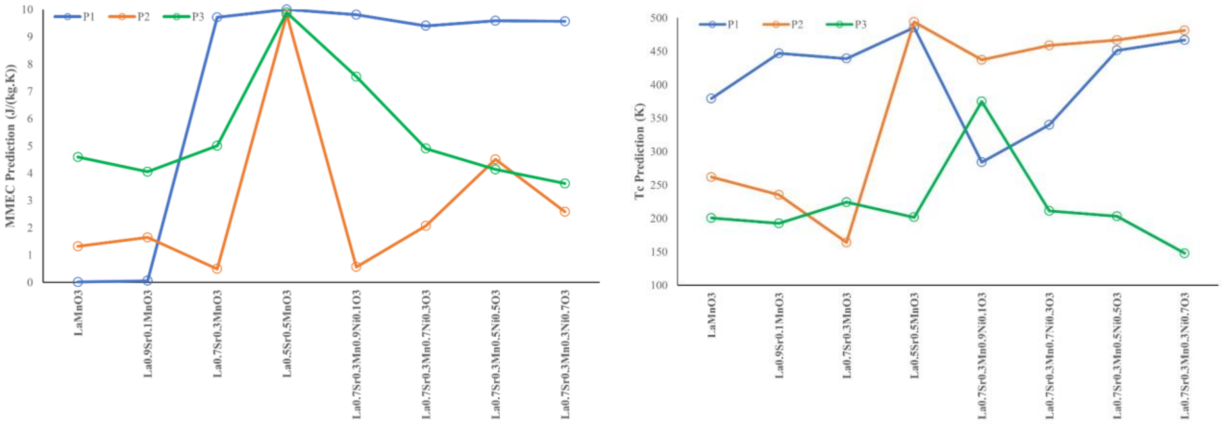

(a) (b)

Fig. 6 Prediction value of (a) Maximum magnetic entropy change and (b) Curie temperature for manganite, using experimental data from Table III

The value of MMEC and Tc predictions for manganite in Table III, as provided by the P1, P2, and P3 models, exhibit observable discrepancies. The presence of divalent Sr results in a rising trend in the MMEC value. The MMEC value observed in $La_{0.5}Sr_{0.5}MnO_3$ exhibits a value that is nearest and comparatively the highest within the three models. Nevertheless, P1's MMEC value exhibits a significant increase when the divalent Sr atomic fraction surpasses 0.1, surpassing the values of other models. However, P2 exhibits a comparatively lower MMEC value in comparison to P3, except for the MMEC value of $La_{0.7}Sr_{0.3}Mn_{0.5}Ni_{0.5}O_3$. When Ni metal is added to manganite, replacing the Mn element, the MMEC value exhibits a distinct trend. Upon observing the P1 model, it is evident that the MMEC value has remained relatively stable, with the MMEC value being the highest among all other models. The P2 model exhibits a rising pattern, albeit with a lower magnitude compared to the P1 model. The P3 model exhibits a reduced MMEC value in comparison to P1, similar to P2. The primary distinction lies in the fact that the MMEC value in the P3 model exhibits a declining pattern while its magnitude surpasses relatively that of the P2 model. The presence of divalent Sr and Ni metals into manganite for P1 and P2 models demonstrates a consistent pattern of higher Tc values. Similar to the MMEC value of $La_{0.5}Sr_{0.5}MnO_3$, the Tc values resulting from the P1 and P2 models are relatively similar and represent the maximum values. The Tc value acquired from the P2 model exhibits a comparatively increased value compared to other models. The presence of Ni metal in the P1 and P2 models of manganite exhibits a comparable trend, wherein the Tc value rises proportionally to the increase in Ni metal substitution. Based on the trend of MMEC and Tc values, it appears that the P1 model shows a roughly equal ratio of MMEC to Tc values, indicating an increase. The P2 model, on the other hand, displays a ratio of increasing MMEC to Tc values that are less than 1. Lastly, the P3 model demonstrates a decline in both MMEC and Tc values with a ratio greater than -1. While there is some variability in the results obtained from models P1, P2, and P3, all three models have shown to have fair predictive capability when determining the MMEC and Tc values of manganite that has been substituted with divalent Sr and Ni metals.

IV. CONCLUSION

From this study, it was found that BPNN can be used in the determination of MMEC and Tc characteristics of manganite. The BPNN is very effective in making predictions, but in the analysis, it is strongly influenced by the accuracy of parameter determination. Using 15 variables consisting of lattice parameters and manganite alloy composition has provided excellent predictions of MMEC and Tc values. However, there are several types of manganites whose predicted values still need to be precise. Processing group P1 with 45 neurons in a single hidden layer provides a very small training RMSE and MAE and RMSE prediction values for MMEC of 0.012 and 0.015 and Tc of 0.022 and 0.021. For processing group P2, it gives MAE and RMSE prediction values for MMEC of 0.014 and 0.010 and Tc of 0.026 and 0.020. While the processing group P3 provides MAE and

RMSE prediction values for MMEC of 0.012 and 0.010 and Tc of 0.025 and 0.020. Considering the accuracy of the values obtained, the use of BPNN has the potential to be applied and show a fair result in predicting an unknown MMEC and Tc characteristic of manganite during conducting the experiments. It has been noticed that the performance of machine learning models can vary depending on the quality of the data used, and this performance can also differ across different case studies. Consequently, it is necessary to conduct an individual examination for each case study. By predicting the desired MMEC and Tc, it is expected to facilitate the design of manganite materials and can reduce research costs.

ACKNOWLEDGEMENT

The authors would like to thank Pamulang University, the Ministry of Education, Culture, Research and Technology, and the National Research and Innovation Agency for their support. This activity is financed through research grant funding from the Ministry of Education, Culture, Research and Technology in 2023 with contract numbers 180/E5/PG.02.00.PL/2023; 021/SP2H/RT-MONO/LL4/2023; 107/D5/SK/LPPM/UNPAM/VII/2023.

REFERENCES

[1] M.-H. Phan and S.-C. Yu, "Review of the magnetocaloric effect in manganite materials," *J. Magn. Magn. Mater.*, vol. 308, no. 2, pp. 325–340, Jan. 2007, doi: 10.1016/j.jmmm.2006.07.025.

[2] T. Gottschall, "Magnetocaloric effect of gadolinium in high magnetic fields," *Phys. Rev. B*, vol. 99, no. 13, p. 134429, Apr. 2019, doi: 10.1103/PhysRevB.99.134429.

[3] L. V. Bau, O. Morán, P. T. Tho, and P. T. Phong, "Critical Properties and Magnetocaloric Effect in La0.7Ba0.3Mn0.8Ti0.2O3 Ceramic," *Metall. Mater. Trans. A*, vol. 51, no. 4, pp. 1924–1932, Apr. 2020, doi: 10.1007/s11661-020-05662-y.

[4] T. Shou, "Degradation of gas-phase o-xylene via combined non-thermal plasma and Fe doped LaMnO3 catalysts: Byproduct control," *J. Hazard. Mater.*, vol. 387, p. 121750, Apr. 2020, doi: 10.1016/j.jhazmat.2019.121750.

[5] F. Li, Z. Wang, A. Wang, S. Wu, and L. Zhang, "N-type LaFe1-xMnxO3 prepared by sol-gel method for gas sensing," *J. Alloys Compd.*, vol. 816, p. 152647, Mar. 2020, doi: 10.1016/j.jallcom.2019.152647.

[6] Z. Xu, Y. Li, Y. Wan, S. Zhang, and C. Xia, "Nickel enriched Ruddlesden-Popper type lanthanum strontium manganite as electrode for symmetrical solid oxide fuel cell," *J. Power Sources*, vol. 425, pp. 153–161, Jun. 2019, doi: 10.1016/j.jpowsour.2019.04.005.

[7] P. Goel, "Perovskite materials as superior and powerful platforms for energy conversion and storage applications," *Nano Energy*, vol. 80, p. 105552, Feb. 2021, doi: 10.1016/j.nanoen.2020.105552.

[8] M. S. Sowmehsaraee, M. Ranjbar, and M. Abedi, "Investigating the effect of nano-structured magnetic particles lanthanum strontium manganite on perovskite solar cells," *J. Sol. Energy Res.*, vol. 7, no. 1, pp. 945–956, 2022, doi: 10.22059/JSER.2021.325062.1205.

[9] A. Khochaiche, "First extensive study of silver-doped lanthanum manganite nanoparticles for inducing selective chemotherapy and radio-toxicity enhancement," *Mater. Sci. Eng. C*, vol. 123, p. 111970, Apr. 2021, doi: 10.1016/j.msec.2021.111970.

[10] F. Kuang, Z. Long, D. Kuang, X. Liu, and R. Guo, "Application of back propagation neural network to the modeling of slump and compressive strength of composite geopolymers," *Comput. Mater. Sci.*, vol. 206, p. 111241, 2022, doi: 10.1016/j.commatsci.2022.111241.

[11] R. Al-Jarrah and F. M. AL-Oqla, "A novel integrated BPNN/SNN artificial neural network for predicting the mechanical performance of green fibers for better composite manufacturing," *Compos. Struct.*, vol. 289, p. 115475, Jun. 2022, doi: 10.1016/j.compstruct.2022.115475.

[12] Y. Wang, "Prediction and Analysis of Tensile Properties of Austenitic Stainless Steel Using Artificial Neural Network," *Metals (Basel).*, vol. 10, no. 2, p. 234, 2020, doi: 10.3390/met10020234.

[13] E. Bouzaiene, A. H. Dhahri, J. Dhahri, E. K. Hlil, and A. Bajahzar, "Effect of A-site-substitution on structural, magnetic and magnetocaloric properties in La0.7Sr0.3 Mn0.9Cu0.1O3 manganite," *J. Magn. Magn. Mater.*, vol. 491, p. 165540, Dec. 2019, doi: 10.1016/j.jmmm.2019.165540.

[14] V. Franco, J. S. Blázquez, and A. Conde, "Field dependence of the magnetocaloric effect in materials with a second order phase transition: A master curve for the magnetic entropy change," *Appl. Phys. Lett.*, vol. 89, no. 22, Nov. 2006, doi: 10.1063/1.2399361.

[15] V. Franco, J. S. Blázquez, J. J. Ipus, J. Y. Law, L. M. Moreno-Ramírez, and A. Conde, "Magnetocaloric effect: From materials research to refrigeration devices," *Prog. Mater. Sci.*, vol. 93, pp. 112–232, Apr. 2018, doi: 10.1016/j.pmatsci.2017.10.005.

[16] L. Lin, "Engineering of hole-selective contact for high-performance perovskite solar cell featuring silver back-electrode," *J. Mater. Sci.*, vol. 54, no. 10, pp. 7789–7797, May 2019, doi: 10.1007/s10853-018-03258-x.

[17] Z. Yang, "Opto-electric investigation for Si/organic heterojunction single-nanowire solar cells," *Sci. Rep.*, vol. 7, no. 1, p. 14575, Nov. 2017, doi: 10.1038/s41598-

017-15300-0.

[18] W. Guo, "Nanostructure surface patterning of GaN thin films and application to AlGaN/AlN multiple quantum wells: A way towards light extraction efficiency enhancement of III-nitride based light emitting diodes," *J. Appl. Phys.*, vol. 117, no. 11, p. 113107, Mar. 2015, doi: 10.1063/1.4915903.

[19] E. Oumezzine, S. Hcini, E.-K. Hlil, E. Dhahri, and M. Oumezzine, "Effect of Ni-doping on structural, magnetic and magnetocaloric properties of La 0.6 Pr 0.1 Ba 0.3 Mn 1− x Ni x O 3 nanocrystalline manganites synthesized by Pechini sol–gel method," *J. Alloys Compd.*, vol. 615, pp. 553–560, Dec. 2014, doi: 10.1016/j.jallcom.2014.07.001.

[20] K. Abdouli, "Structural, magnetic and magnetocaloric properties of La0.5Sm0.2Sr0.3Mn1-xFexO3 compounds with (0 ≤ x ≤ 0.15)," *J. Magn. Magn. Mater.*, vol. 475, pp. 635–642, Apr. 2019, doi: 10.1016/j.jmmm.2018.12.007.

[21] M. Oumezzine, S. Zemni, and O. Peña, "Room temperature magnetic and magnetocaloric properties of La0.67Ba0.33Mn0.98Ti0.02O3 perovskite," *J. Alloys Compd.*, vol. 508, no. 2, pp. 292–296, Oct. 2010, doi: 10.1016/j.jallcom.2010.08.145.

[22] S. E. Kossi, S. Ghodhbane, S. Mnefgui, J. Dhahri, and E. K. Hlil, "The impact of disorder on magnetocaloric properties in Ti-doped manganites of La0.7Sr0.25Na0.05Mn(1−x)TixO3 (0≤x≤0.2)," *J. Magn. Magn. Mater.*, vol. 395, pp. 134–142, Dec. 2015, doi: 10.1016/j.jmmm.2015.07.050.

[23] A. Selmi, R. M'nassri, W. Cheikhrouhou-Koubaa, N. Chniba Boudjada, and A. Cheikhrouhou, "Influence of transition metal doping (Fe, Co, Ni and Cr) on magnetic and magnetocaloric properties of Pr0.7Ca0.3MnO3 manganites," *Ceram. Int.*, vol. 41, no. 8, pp. 10177–10184, Sep. 2015, doi: 10.1016/j.ceramint.2015.04.123.

[24] S. Banik, K. Das, and I. Das, "Enhancement of magnetoresistance and magnetocaloric effect at room temperature in polycrystalline Pr0.8-xLaxSr0.2MnO3 (x= 0.2) compound," *J. Magn. Magn. Mater.*, vol. 490, p. 165443, Nov. 2019, doi: 10.1016/j.jmmm.2019.165443.

[25] A. Selmi, R. M'nassri, W. Cheikhrouhou-Koubaa, N. C. Boudjada, and A. Cheikhrouhou, "The effect of Co doping on the magnetic and magnetocaloric properties of Pr0.7Ca0.3Mn1−xCoxO3 manganites," *Ceram. Int.*, vol. 41, no. 6, pp. 7723–7728, Jul. 2015, doi: 10.1016/j.ceramint.2015.02.103.

[26] P. Nisha, S. Savitha Pillai, M. R. Varma, and K. G. Suresh, "Critical behavior and magnetocaloric effect in La0.67Ca0.33Mn1−xCrxO3 (x = 0.1, 0.25)," *Solid State Sci.*, vol. 14, no. 1, pp. 40–47, Jan. 2012, doi: 10.1016/j.solidstatesciences.2011.10.013.

[27] J. Makni-Chakroun, R. M'nassri, W. Cheikhrouhou-Koubaa, M. Koubaa, N. Chniba-Boudjada, and A. Cheikhrouhou, "Effect of A-site deficiency on investigation of structural, magnetic and magnetocaloric behaviors for (LaSr)-lacunar manganites," *Chem. Phys. Lett.*, vol. 707, pp. 61–70, Sep. 2018, doi: 10.1016/j.cplett.2018.07.039.

[28] Z. Wang and J. Jiang, "Magnetic entropy change in perovskite manganites La0.7A0.3MnO3 La0.7A0.3Mn0.9Cr0.1O3 (A = Sr, Ba, Pb) and Banerjee criteria on phase transition," *Solid State Sci.*, vol. 18, pp. 36–41, Apr. 2013, doi: 10.1016/j.solidstatesciences.2012.12.020.

[29] A. Selmi, R. M'nassri, W. Cheikhrouhou-Koubaa, N. Chniba Boudjada, and A. Cheikhrouhou, "Effects of partial Mn-substitution on magnetic and magnetocaloric properties in Pr0.7Ca0.3Mn0.95X0.05O3 (Cr, Ni, Co and Fe) manganites," *J. Alloys Compd.*, vol. 619, pp. 627–633, Jan. 2015, doi: 10.1016/j.jallcom.2014.09.078.

[30] E. Tka, K. Cherif, and J. Dhahri, "Evolution of structural, magnetic and magnetocaloric properties in Sn-doped manganites La0.57Nd0.1Sr0.33Mn1−x Sn x O3 (x = 0.05–0.3)," *Appl. Phys. A*, vol. 116, no. 3, pp. 1181–1191, Sep. 2014, doi: 10.1007/s00339-013-8202-5.

[31] A. Bettaibi, "Effect of chromium concentration on the structural, magnetic and electrical properties of praseodymium-calcium manganite," *J. Alloys Compd.*, vol. 650, pp. 268–276, Nov. 2015, doi: 10.1016/j.jallcom.2015.05.161.

[32] S. Vadnala and S. Asthana, "Magnetocaloric effect and critical field analysis in Eu substituted La 0.7-x Eu x Sr 0.3 MnO 3 (x = 0.0, 0.1, 0.2, 0.3) manganites," *J. Magn. Magn. Mater.*, vol. 446, pp. 68–79, Jan. 2018, doi: 10.1016/j.jmmm.2017.09.001.

[33] S. Kallel, N. Kallel, O. Peña, and M. Oumezzine, "Large magnetocaloric effect in Ti-modified La0.70Sr0.30MnO3 perovskite," *Mater. Lett.*, vol. 64, no. 9, pp. 1045–1048, May 2010, doi: 10.1016/j.matlet.2010.02.005.

[34] S. Hcini, M. Boudard, S. Zemni, and M. Oumezzine, "Effect of Fe-doping on structural, magnetic and magnetocaloric properties of Nd0.67Ba0.33Mn1−xFexO3 manganites," *Ceram. Int.*, vol. 40, no. 10, pp. 16041–16050, Dec. 2014, doi: 10.1016/j.ceramint.2014.07.140.

[35] A. O. Ayaş, S. Kılıç Çetin, M. Akyol, G. Akça, and A. Ekicibil, "Effect of B site partial Ru substitution on structural magnetic and magnetocaloric properties in La0.7Pb0.3Mn1-xRuxO3 (x = 0.0, 0.1 and 0.2) perovskite system," *J. Mol. Struct.*, vol. 1200, p. 127120, Jan. 2020, doi: 10.1016/j.molstruc.2019.127120.

[36] S. Mahjoub, M. Baazaoui, R. M'nassri, H. Rahmouni, N. C. Boudjada, and M. Oumezzine, "Effect of iron substitution on the structural, magnetic and magnetocaloric properties of Pr0.6Ca0.1Sr0.3Mn1−xFexO3 (0⩽x⩽0.075) manganites," *J. Alloys Compd.*, vol. 608, pp. 191–196, Sep. 2014, doi: 10.1016/j.jallcom.2014.04.125.

[37] H. Ben Khlifa, Y. Regaieg, W. Cheikhrouhou-Koubaa, M. Koubaa, and A. Cheikhrouhou, "Structural, magnetic and magnetocaloric properties of K-doped Pr0.8Na0.2−xKxMnO3 manganites," *J. Alloys Compd.*, vol. 650, pp. 676–683, Nov. 2015, doi: 10.1016/j.jallcom.2015.07.140.

[38] C. G. Ünlü, Y. E. Tanış, M. B. Kaynar, T. Şimşek, and Ş. Özcan, "Magnetocaloric effect in La0.7 NdxBa(0.3-x)MnO3 (x = 0, 0.05, 0.1) perovskite manganites," *J. Alloys Compd.*, vol. 704, pp. 58–63, May 2017, doi: 10.1016/j.jallcom.2017.02.030.

[39] A. Mleiki, S. Othmani, W. Cheikhrouhou-Koubaa, M. Koubaa, A. Cheikhrouhou, and E. K. Hlil, "Effect of praseodymium doping on the structural, magnetic and magnetocaloric properties of Sm0.55−xPrxSr0.45MnO3 (0.1⩽x⩽0.4) manganites," *J. Alloys Compd.*, vol. 645, pp. 559–565, Oct. 2015, doi: 10.1016/j.jallcom.2015.05.043.

[40] A. Ben Jazia Kharrat, K. Khirouni, and W. Boujelben, "Structural, magnetic, magnetocaloric and impedance spectroscopy analysis of Pr0.8Sr0.2MnO3 manganite prepared by modified solid-state route," *Phys. Lett. A*, vol. 382, no. 48, pp. 3435–3448, Dec. 2018, doi: 10.1016/j.physleta.2018.10.010.

[41] S. Kallel, N. Kallel, A. Hagaza, O. Peña, and M. Oumezzine, "Large magnetic entropy change above 300 K in (La0.56Ce0.14)Sr0.3MnO3 perovskite," *J. Alloys Compd.*, vol. 492, no. 1–2, pp. 241–244, Mar. 2010, doi: 10.1016/j.jallcom.2009.11.107.

[42] A. Rostamnejadi, M. Venkatesan, P. Kameli, H. Salamati, and J. M. D. Coey, "Magnetocaloric effect in La0.67Sr0.33MnO3 manganite above room temperature," *J. Magn. Magn. Mater.*, vol. 323, no. 16, pp. 2214–2218, Aug. 2011, doi: 10.1016/j.jmmm.2011.03.036.

[43] H. Ben Khlifa, "Effect of K-doping on the structural, magnetic and magnetocaloric properties of Pr0.8Na0.2–K MnO3 (0 ≤ x ≤ 0.15) manganites," *J. Alloys Compd.*, vol. 680, pp. 388–396, Sep. 2016, doi: 10.1016/j.jallcom.2016.04.138.

[44] K. Laajimi, M. Khlifi, E. K. Hlil, M. H. Gazzah, and J. Dhahri, "Enhancement of magnetocaloric effect by Nickel substitution in La0.67Ca0.33Mn0.98Ni0.02O3 manganite oxide," *J. Magn. Magn. Mater.*, vol. 491, p. 165625, Dec. 2019, doi: 10.1016/j.jmmm.2019.165625.

[45] Y. Zhang and X. Xu, "Machine learning the magnetocaloric effect in manganites from lattice parameters," *Appl. Phys. A*, vol. 126, no. 5, 2020, doi: 10.1007/s00339-020-03503-8.

[46] T.-A. Nguyen, H.-B. Ly, and B. T. Pham, "Backpropagation Neural Network-Based Machine Learning Model for Prediction of Soil Friction Angle," *Math. Probl. Eng.*, vol. 2020, pp. 1–11, Dec. 2020, doi: 10.1155/2020/8845768.

[47] A. F. Daru, M. B. Hanif, and E. Widodo, "Improving Neural Network Performance with Feature Selection Using Pearson Correlation Method for Diabetes Disease Detection," *JUITA J. Inform.*, vol. 9, no. 1, p. 123, May 2021, doi: 10.30595/juita.v9i1.9941.

[48] A. G. Priya Varshini, K. Anitha Kumari, D. Janani, and S. Soundariya, "Comparative analysis of Machine learning and Deep learning algorithms for Software Effort Estimation," *J. Phys. Conf. Ser.*, vol. 1767, no. 1, p. 012019, 2021, doi: 10.1088/1742-6596/1767/1/012019.